sustainability

MDPI

Article

Assessment of Water Flow Glazing as Building-Integrated Solar Thermal Collector

Fernando del Ama Gonzalo [1,*], Belén Moreno Santamaría [2] and Juan A. Hernández Ramos [3]

[1] Department of Sustainable Product Design and Architecture, Keene State College, 229 Main St., Keene, NH 03435, USA
[2] Department of Construction and Architectural Technology, Technical School of Architecture of Madrid, Universidad Politécnica de Madrid, Av. Juan de Herrera, 4, 28040 Madrid, Spain
[3] Department of Applied Mathematics, School of Aeronautical and Space Engineering, Universidad Politécnica de Madrid, Plaza Cardenal Cisneros 3, 28040 Madrid, Spain
* Correspondence: fernando.delama@keene.edu

Abstract: In buildings with ambitious energy goals or limited roof areas for on-site energy generation, building-integrated solar thermal collectors are one of the main strategies to provide on-site renewable energy to the built environment. In addition, designing large glazing facades is a challenge to achieving the goal of zero-energy buildings due to the thermal load produced by standard double or triple glazing. This research shows that Water Flow Glazing (WFG) can produce domestic hot water as a building-integrated solar thermal collector by flowing water through the chamber between glass panes and can help reduce thermal loads through facades. In this article, the solar collector's efficiency was defined according to the UNE-EN 12975-2 standard and then applied to the Water Flow Glazing. As a result, the transparent Water Flow Glazing's optical efficiency η_0 varies from 0.648 to 0.742, whereas the thermal loss coefficient a_1 ranges from 9.51 to 4.16. Those values are like those of commercial plate collectors. Afterward, the model to predict the efficiency of WFG was tested in an existing facility by calculating the Normalized Root Mean Square Error (NRMSE) to assess the deviations between the simulation and measured values. Using building-integrated solar collectors can improve the integration of renewable energies in facades and roofs but also increase the uncertainties that affect their efficiencies, such as internal heat loads and heating, cooling, and ventilation systems. Therefore, testing existing facilities can help understand the impact of these technologies in the Zero Energy Building paradigm.

Keywords: water flow glazing; building integrated solar thermal collectors; thermal simulation

Citation: del Ama Gonzalo, F.; Moreno Santamaría, B.; Hernández Ramos, J.A. Assessment of Water Flow Glazing as Building-Integrated Solar Thermal Collector. *Sustainability* **2023**, *15*, 644. https://doi.org/10.3390/su15010644

Academic Editor: Diego Vergara

Received: 1 December 2022
Revised: 27 December 2022
Accepted: 28 December 2022
Published: 30 December 2022

1. Introduction

The increasing use of renewable energy sources through the Energy Performance of Buildings Directive (EPBD) has led to a critical role of solar thermal systems and photovoltaic panels in buildings [1]. By integrating solar systems, building designers contribute to electricity and hot water supply. However, efficiency and reliability affect the market approval of solar systems [2]. Building designers might want solar thermal collectors to be either invisible or appealing and can be integrated into buildings' facades or roofs. In any case, solar collectors must be perceived as an architectural feature of the building design [3]. Passive solar systems have shown a good performance when it comes to building integration. They use solar energy directly to warm up indoor air. Greenhouses are glazed buildings or parts of buildings that let the Sun enter but do not allow the heat to escape, so they manage to keep indoor temperatures higher than outdoors, even in cold environments. On the other hand, active solar systems collect and transform solar radiation into thermal or electric energy for its use in buildings. Solar thermal systems produce thermal energy and accumulate hot water for different uses. Solar photovoltaic panels produce electric energy [4,5].

A thermal solar installation consists of a device exposed to solar radiation that allows the exchange of heat with a conduit to circulate a working fluid which increases its temperature. This fluid, usually water or glycol, can be used for heating devices, swimming pools, or domestic hot water [6]. In addition to being technically feasible, solar thermal collectors must meet other requirements, such as innovative design and size flexibility. Finally, the cost assessment must show relevant savings over the system's life [7]. There are three kinds of solar collectors available in the market: plate, concentration, and vacuum-pipe collectors [8,9]. Plate collectors include pipes where the fluid flows, a heat accumulator (a steel or copper panel crossed by the pipes), and a glass panel that allows the direct solar radiation in but does not let reflected radiation out so that the environment between the glass and the accumulator remains hot. In addition, thermal insulation is placed underneath the accumulator to prevent heat losses, and antifreeze is added to the water to prevent freezing in winter conditions [10]. Concentration collectors use mirrors that reflect the solar radiation and concentrate the sun's rays on a segment of a straight line or a single point, heating a flowing fluid above 100 °C [11]. Vacuum-pipe collectors are made of two concentrical glass pipes with a vacuum between them. The inner glass pipe acts as an absorber, has a round shape, and is filled with a fluid that evaporates exposed to solar radiation. Then, by transmitting the heat to the top part of the pipe, the fluid condenses and goes back to the bottom. Since the vacuum is the best insulator, the absorber has no heat losses, and the collector's efficiency is higher than in plate collectors [12]. Although the goal of solar collectors is to take advantage of solar radiation to raise the temperature of a fluid, flat solar and vacuum pipe collectors do so differently [13]. Flat solar collectors were the first solar devices available on the market; Vacuum pipe technology emerged with different components and increased efficiency. Solar collectors are connected to the Domestic Hot Water (DHW) tank or the heating system by two different layouts: indirect or direct solar thermal systems [14]. The former uses pressurized glycol through the collectors, so water is not exposed to outdoor conditions to avoid freezing, and the heat is transferred using heat exchangers. The latter circulates water directly through solar collectors before entering a buffer tank. Direct solar thermal systems eliminate inefficiencies related to heat exchangers. In addition, water transfers heat better than glycol. However, direct systems must not be used in facilities exposed to freezing temperatures [12].

Although the building industry has offered integrated solar collectors in facades for decades, this system has not become mainstream, and scientific literature has reported very few studies. Some authors analyzed active water glazing systems and compared them with conventional flat plate collectors [15]. Other authors studied solar water glazing without thermal insulation between collectors and walls and stated that the circulating water stream could remove 75% of the absorbed solar heat [16]. Other important aspects of integrated solar collectors without thermal insulation are the efficiency and the influence of warm water in the facade on indoor temperature. Some experimental studies reported that indoor temperature increased less than 1 °C when the water glazing facade removed 50% of incident solar radiation [17,18]. Water Flow Glazing (WFG) is a new building envelope system that can work as building-integrated solar thermal collectors and lower the cooling loads in the summer [19,20]. With traditional double glazing, part of the solar thermal radiation impinges the building envelope and is reflected outdoors. Another part is transmitted indoors. In contrast, using WFG, most non-reflected solar energy is absorbed into the circulating water, and the rest is transmitted inside. In addition, the water can also absorb the internal loads of the room [21,22]. Traditional solar collectors and Water Flow Glazing can circulate a fluid to be heated by the effect of solar radiation. However, there are some differences between the two systems, especially related to the conduit through which water circulates and insulation. For example, there is no duct in Water flow Glazing because the space between glasses exerts this role [23]. Flat solar collectors are usually insulated. In contrast, Water flow Glazing does not have opaque insulation because they are designed to allow the entry of light and thermal energy from the Sun into the buildings [24]. The regulations for thermal solar collectors require that the operating temperature be higher

than 50 °C; otherwise, there is a risk of legionellosis. However, in Water Flow Glazing in façades, the temperatures reached in the circulating water are not so high, so there must be other configurations that absorb a large amount of energy [25,26].

This study aims to analyze the possible application of Water Flow Glazing panels as thermal solar collectors to obtain a first approximation of this type of glazing's efficiency.

In this article, the performance parameters of WFG as building-integrated solar collectors have been defined according to the UNE-EN 12975-2 standard. Secondly, the algebraic equations of a model to assess the water heat absorption of WFG as a solar collector have been explained. Thirdly, the simulation results were compared with actual values measured in a real facility with a WFG curtain wall. Next, the Normalized Root Mean Square Error (NRMSE) was used to assess the deviations between simulation and actual values. Finally, the f-chart method was used to compare the yearly hot water production of the tested facility with the performance of commercial solar collectors. Then, the cost of commercial flat plate collectors and building-integrated Water Flow Glazing was compared to produce the same amount of domestic hot water.

2. Materials and Methods

Flat plate collectors consist of a heat-absorbing plate made of copper or aluminum chemically tinted in black to absorb as much solar radiation as possible. An air gap between the plate and glazing material prevents the heat from being radiated back into the atmosphere. Flat plate collectors can heat the fluid through direct or diffuse sunlight. The outlet temperature of the circulating fluid depends on the amount of solar radiation and the mass flow rate of the fluid that flows through the collectors [4]. Vacuum pipes are made of two layers of glass with a vacuum in between the layers. The outermost layer is Borosilicate glass with a low iron percentage, allowing 98% of solar radiation to pass through. The second inner layer has low-emissivity coatings to reduce losses due to thermal re-irradiation [12]. In this way, vacuum pipes address the three mechanisms that can produce heat losses: convection and conduction, because of the vacuum, and radiation, thanks to the low-emissivity coating. The solar radiation is transmitted to a heat transfer fluid within the tube, which quickly heats up and rises to the top, where the condenser is located. The contact with the cold source causes the condensation of the liquid, which yields its latent heat of vaporization. The great advantage of vacuum tubes is their superior efficiency, especially on cold, windy, or cloudy days. The following sections show the standard procedures to characterize the efficiency of solar collectors to set the basis for assessing the performance of Water Flow Glazing as water-heater devices.

2.1. Performance of Thermal Collectors

The UNE-EN 12975-2 standard defines the performance of all thermal solar collectors manufactured and marketed in Spain [27]. The main characteristic specified in this standard is the solar collector efficiency, η given by Equation (1).

$$\eta = \frac{\dot{Q}}{Ai_0} = \eta_0 - a_1(T_{m,e}) - a_2 i_0 (T_{m,e})^2, \quad (1)$$

where $\dot{Q}$ is the thermal power absorbed by the fluid, i_0 is the solar irradiance, and A is the area of absorption, Ai_0 is the incident solar energy, η_0 is the optical efficiency of the collector, and $T_{m,e}$ is the reduced temperature difference, given by Equation (2).

$$T_{m,e} = \frac{(T_m - T_{ext})}{i_0}, \quad (2)$$

where T_m is the average temperature of the fluid in the collector and T_{ext} is the average temperature of the ambient air. Thus, the definition of performance is usually expressed as in Equation (3).

$$\eta = \eta_0 - a_1\left(\frac{T_m - T_{ext}}{i_0}\right) - a_2\left(\frac{(T_m - T_{ext})^2}{i_0}\right). \quad (3)$$

Figure 1 shows the efficiency of a standard solar thermal collector as a function of the temperature difference $(T_m - T_{ext})$ when the solar irradiance, i_0 is 1000 (W/m^2). For commercial solar collectors, the value of the optical efficiency, η_0, ranges between 0.7 and 0.8. Furthermore, the loss coefficient a_1 is usually between 1 and 4, while a_2 oscillates between 5×10^{-3} and 20×10^{-3} [28]. Therefore, the collectors' performance is almost linear, and the quadratic term has little influence.

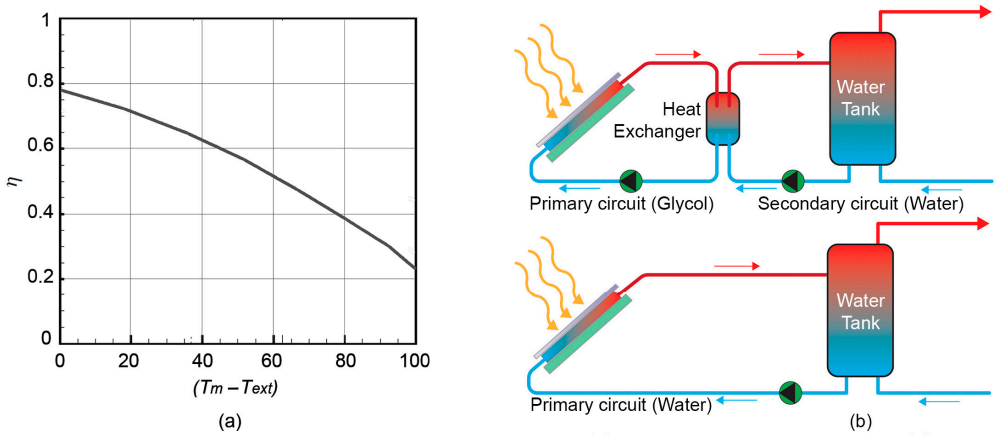

Figure 1. (**a**) Efficiency of a standard solar thermal collector as a function of the temperature difference $(T_m - T_{ext})$ when i_0 is 1000 (W/m^2); (**b**) Schematic views of direct and indirect solar thermal systems.

The area of absorption is defined in ISO 9488 [29] as the area of the surface intended to absorb solar radiation. For vacuum pipe collectors, it depends on the diameter of the cylinder formed by the absorbing material and not on the diameter of the glass tubes. Sometimes, in the definition of performance, the opening area is used instead of the absorption area. The opening area is defined as the surface area where solar radiation is admitted to the collector. For vacuum collectors, it depends on the diameter of the glass tubes. In the case of flat collectors, absorption and opening areas are very similar [30]. One of the most common issues for solar collectors defined by ISO 9488 is the stagnation temperature, which is the temperature reached by the fluid when it is not running through the collector [31]. A high stagnation temperature is a significant problem associated with solar thermal installations. Hence, the fluid must circulate inside the solar collectors at all times, even if removing energy is unnecessary [32]. Part of the solar energy impinging the panel is reflected or absorbed but immediately re-irradiated, which decreases the optical efficiency of the collector η_0. Besides, there are heat losses because the average temperature of the fluid, T_m, is higher than the average temperature of the outside ambient air T_{ext}. So, there is an exchange of heat by convection and radiation between the solar collector and the environment, reducing the use of the incident solar energy. It is necessary to calculate the coefficients a_1 and a_2 by means of experimental tests to obtain the efficiency in each collector. Since the terms of Equation (3) proportional to these coefficients represent losses, a_1 and a_2 must be positive. If, as a result of the tests, a_2 were a negative value, the UNE-EN 12975-2 standard specifies that the value of a_2 must be equal to 0. Figure 2 compares the efficiency of two collector types available in the market. It shows that if the value of $((T_m - T_{ext})/i_0)$ increases, the behavior of vacuum pipe solar collectors is much better than that of flat solar collectors. Figure 2 highlights two cases when the outdoor temperature is fixed at 10 °C and 30 °C. Assuming that the heat transfer liquid temperature remains constant at 60 °C, the efficiency of the vacuum pipe collector is higher for both cases. The intersection point

of the two curves happens when $((T_m - T_{ext})/i_0) = 0.026$, so if the temperature difference between the fluid circulating through the collector and the outdoor temperature is higher than 21 °C, the performance of the vacuum tube collector will be better. The efficiency of vacuum pipes is much higher as the outdoor temperature gets colder. However, the optical efficiency, η_0, which corresponds with the vertical line at the origin, is higher for flat panels, mainly due to the use of the entire exterior surface occupied by the glass and the greenhouse effect in the inner chamber.

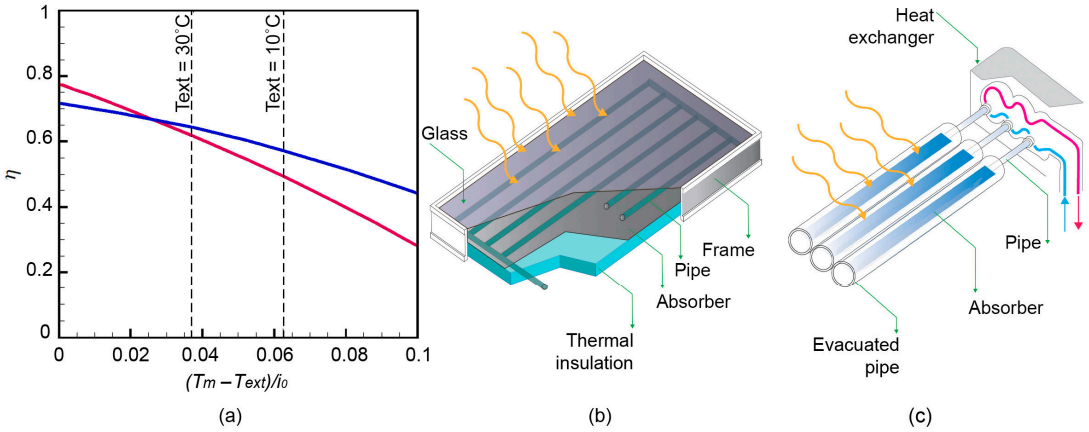

Figure 2. (**a**) Comparison of the performance of a flat solar collector Disol Satius 22 L Plus (red curve) with that of a vacuum pipe collector Thermomax DF100 (blue curve) when incident solar radiation i_0 is 800 (W/m^2); (**b**) Flat collectors; (**c**) Vacuum pipe collectors.

Table 1 shows that the optical efficiency, η_0 is better in flat solar collectors, whereas vacuum pipe ones reduce their coefficient of losses a_1, a_2 which decisively influences the solar panel's efficiency. The Thermomax DF100 has a very high optical efficiency η_0 because of a new fluid circulation coaxial system that improves the insulation and increases the vacuum in the pipes.

Table 1. Values of the optical efficiency and of the coefficients of thermal losses for three solar collectors available in the market.

Collector Type	Model [1]	η_0	a_1	a_2
Flat plate	Disol Satius 22 L Plus	0.775	3.73	0.0152
Vacuum-pipe	Thermomax DF100	0.781	1.44	0.0062

[1] Values taken from Appendix A.

2.2. Water Flow Glazing as a Solar Collector

According to the spectral and thermal behavior of Water Flow Glazing [33], the efficiency is a function of the heat absorbed by the circulating fluid and the solar radiation per square meter impinging on the glazing, i_0. The definition of efficiency in Equation (3) can be applied to Water Flow Glazing to determine its performance as a solar collector. Figure 3 illustrates the parameters used for the calculation of the WFG performance.

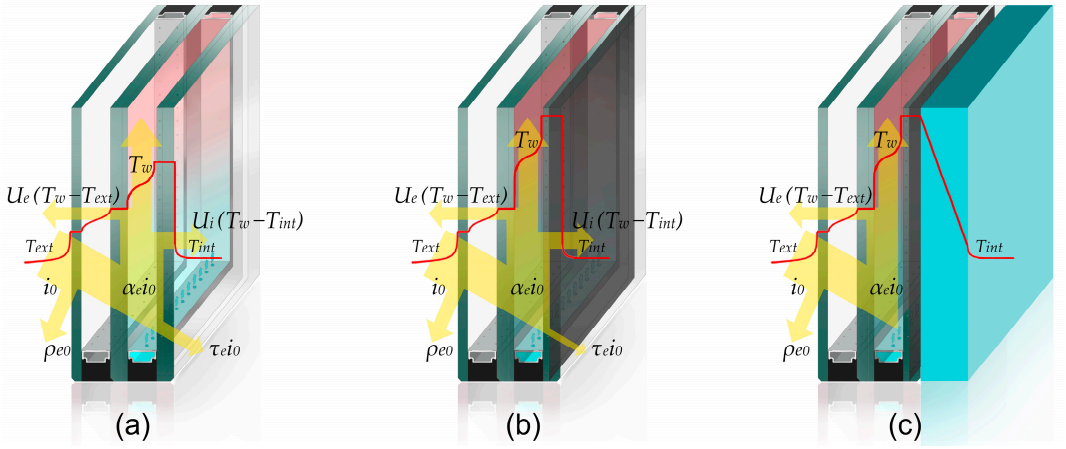

Figure 3. Schematic view of heat flows and temperature distribution in Water Flow Glazing; (**a**) Transparent WFG; (**b**) WFG with PVB interlayer; (**c**) WFG with thermal insulation.

The thermal resistances from the water chamber to the outdoor air were added up to calculate the thermal resistance $1/U_e$, as it is shown in Equation (4).

$$\frac{1}{U_e} = \frac{1}{h_e} + \frac{1}{h_g} + \frac{1}{h_w}, \tag{4}$$

where h_e, h_g, h_w are the convective heat coefficients of the outdoor air layer, in the gas cavity, and in the fluid layer, respectively. The thermal resistance from the water chamber to the indoor air $1/U_i$, is shown in Equation (5), where h_i is the convective heat coefficient of the indoor air layer.

$$\frac{1}{U_i} = \frac{1}{h_i} + \frac{1}{h_w}, \tag{5}$$

The incident radiation i_0, has a reflected component, $\rho_e i_0$, a transmitted component, $\tau_e i_0$, and an absorbed component, $\alpha_e i_0$. Equation (6) shows that the heat absorbed by the fluid can be related to the solar radiation absorbed by the glazing, $\alpha_e i_0$, and heat flows between the Water Flow Glazing, outdoors and indoors. Most of the absorbed incident radiation is absorbed by the flowing water and the rest is re-emitted outdoors or indoors, $q_e i_0$ and $q_i i_0$, respectively. Finally, $U_e(T_{ext} - T_w)$ is the heat transfer by convection and radiation due to temperature differences between water and the outdoor temperature, and $U_i(T_{int} - T_w)$ is due to temperature differences between water and the indoor temperature.

$$\eta = \frac{\alpha_e i_0 - [U_e(T_w - T_{ext}) + q_e i_0] - [U_i(T_w - T_{int}) + q_i i_0]}{i_0}, \tag{6}$$

where U_i and U_e are the thermal transmittances to the interior and exterior, respectively, T_w is the average water temperature in the Water Flow Glazing, T_{ext} is the average outdoor temperature, and T_{int} is the average indoor temperature. Equation (7) results from developing Equation (6).

$$\eta = (\alpha_e - q_i - q_e) - U_e\frac{(T_w - T_{ext})}{i_0} - U_i\frac{(T_w - T_{int})}{i_0}, \tag{7}$$

where the net absorption factor of solar energy, $(\alpha_e - q_i - q_e)$ that occurs in the Water Flow Glazing is the final absorption of energy in a steady state when the working fluid is at the same temperature as the exterior and interior environment, $T_w = T_{ext} = T_{int}$. When comparing Equation (3) with Equation (7), $(\alpha_e - q_i - q_e)$ is equivalent to the optical efficiency of the collector η_0. The first difference between the ISO model for solar collectors and the proposed WFG is the absence of a quadratic term in Equation (7) due to considering a linear thermal model for the resolution of the heat transfer problem in glazing. A second-order

non-linear effect associated with the heat exchanges by convection and radiation between the active glazing and indoor and outdoor environments has not been considered. U_e, U_i, and α_N were constant for Water Flow Glazing setting the water temperature, T_w, at 60 °C, outdoor temperature, T_{ext}, at 30 °C, and indoor temperature, T_{int}, at 25 °C. The second difference is the factor that multiplies the thermal transmittance, U_i, which involves the temperature difference between the circulating fluid, T_w, and the indoor temperature, T_{int}. There is no equivalency for plate collectors since they have thermal insulation on the side that is not exposed to the sun.

3. Results

Throughout this section, it will be assumed that the temperature of the fluid through Water Flow Glazing, T_w when it works as a solar thermal collector is 60 °C, the outdoor temperature, T_{ext} is 30 °C, and the indoor temperature T_{int} is 25 °C. Working with high fluid temperatures can affect heat transfer by convection and radiation in closed cavities. The models for heat transfer set out in ISO 15099:2003 will be used [34], with a glazing height of 1 m.

3.1. Water Flow Glazing with Thermal Insulation on the Indoor Layer (U_i = 0)

If WFG has thermal insulation on the interior face, the same conditions presented for the plate and vacuum-pipe collectors will be considered. If thermal transmittance, U_i is 0, then the convection coefficient, h_i, and the re-emitted heat flow towards inside, q_i, are zero, too. The following subsections describe the impact of different glazing configurations under this hypothesis.

3.1.1. The Effect of Insulating Air Chambers

Reducing the coefficient of thermal losses is especially important to increase the efficiency of the solar collector [35]. In Equation (3), the coefficient of thermal losses a_1 can be compared with U_e in Equation (7). It is convenient to add insulating air chambers to reduce the thermal transmittance, U_e, to the outside and, therefore, to increase efficiency. On the other hand, by adding the air chamber, the coefficient of re-emission to the outside, q_e, increases, which reduces the optical efficiency of the collector, η_0. The air chamber also increases the number of reflections, which impacts the optical efficiency, η_0, by increasing the direct reflex factor, ρ_e, and thus reducing the equivalent absorptance, α_e. Equation (7) has been used to evaluate the effect of the air chamber on thermal transmittance. Table 2 compares U_e, the thermal emission coefficient, q_e, and the optical efficiency for double and triple Water Flow Glazing with 45° tilts. The selected triple Water Flow Glazing was made of an exterior 4 mm glass pane, an air chamber, and two laminated glasses (4+4 mm) with a water chamber.

Table 2. Comparison of the optical efficiency of the collector, η_0, thermal transmittance to the outside, U_e, and coefficient of thermal re-emission to the outside, q_e.

Glazing	η_0	U_e (W/m^{2}K)	q_e (W/m^2)
4+4/Water/4+4	0.462	19.28	0.040
4/Air/4+4/Water/4+4	0.411	5.83	0.093

Triple Glazing parameters as a solar collector show better performance because the decrease in U_e is much more significant than the decrease in the optical efficiency η_0 and the increase of thermal re-emission factor q_e, so the effect of reflections in the air chamber does not seem relevant.

3.1.2. The Effect of Low Emissivity Coatings

Low emissivity coatings reduce the thermal coefficient, h_c of air cavities in transparent glazing [36]. Therefore, they can help decrease the thermal transmittance to outdoor U_e.

Coatings do not absorb radiation, so the only effect is due to the low emissivity. Table 3 compares U_e, the thermal emission coefficient, q_e, and the optical efficiency η_0 for different low emissivity coatings in triple Water Flow Glazing (4/Air/4+4/Water/4+4) with 45 tilts. The coating was applied on the interior face of the air cavity. The emissivity of glasses without coatings, ε, is 0.837, whereas low emissivity coatings have values of 0.10 and 0.01, respectively. A low-emissive treatment on one of the chamber surfaces reduces the U_e coefficient, equivalent to the loss coefficient a_1, while the optical efficiency η_0 does not change considerably.

Table 3. Comparison of the optical efficiency of the collector, η_0, thermal transmittance to the outside, U_e, and coefficient of thermal re-emission to the outside, q_e for triple Water Flow Glazing with low emissivity coatings.

ε_1 [1]	ε_2 [1]	η_0	U_e (W/m^{2}K)	q_e (W/m^2)
0.837	0.837	0.411	5.83	0.093
0.837	0.10	0.406	3.69	0.098
0.837	0.01	0.405	3.33	0.099

[1] ε_1 is the emissivity of the outdoor glass pane and ε_2, of the indoor glass pane.

The small changes in η_0 are due to the thermal reemission factor outdoors, q_e, since for all cases, both the equivalent absorption α_e and the thermal reemission factor indoors, q_i are the same.

3.1.3. The Effect of Polyvinyl Butyral (PVB) Layers

Polyvinyl butyral is a resin used for glass panels that require strong binding. PVB layers can be manufactured in colored or transparent sheets for architectural laminated glass. The PVB increases the impact resistance of the glazing and can affect its optical and thermal properties [37]. The darker a butyral layer, the greater the amount of radiant energy it can absorb [38]. Table 4 shows the results of the optical efficiency of the collector η_0 and the coefficient of thermal losses a_1 for different possible PVB layers. The coefficient of losses, a_1 varies because different amounts of radiation are absorbed by changing the type of PVB. In addition, energy absorption changes the temperatures of interfaces and, therefore, small changes in the convection coefficient h_c occur.

Table 4. Comparison of the solar absorption, the g-factor, the optical efficiency of the collector, η_0, and the coefficient of losses, a_1 for triple Water Flow Glazing with different PVB layers.

PVB Layer [1]	Solar Absorption	g	η_0	a_1 (W/m^{2}K)
Transparent			0.405	3.41
000H	32.7	0.69	0.483	3.42
003H	44.1	0.64	0.675	3.43
07AH	61	0.57	0.778	3.42

[1] Data available in [39].

Triple Water Flow Glazing (4/Air/4+4/Water/4+4) with 45° tilts has been tested with different PVB layers, from single transparent to 07AH, with the darkest color and lower visual transmittance.

3.2. Transparent Water Flow Glazing

This section analyzed the behavior of transparent WFG as a transparent envelope and its ability to heat up water, integrated into facades, and skylights. If WFG does not have thermal insulation on the interior face, then the convection coefficient, h_i, and the re-emitted heat flow towards inside, q_i, are not zero. The following subsections describe

the impact of different glazing configurations under this hypothesis. On the one hand, the WFG as a solar collector is influenced by the thermal transmittance U_i. On the other hand, as a part of the building's glazed envelope. It is characterized by the visible transmittance τ_v and the g-factor. Equation (8) results from developing Equation (7) considering the U_i thermal transmittance.

$$\eta = (\alpha_e - q_i - q_e) - \left(U_e + U_i \frac{(T_w - T_{int})}{(T_w - T_{ext})}\right) \frac{(T_w - T_{ext})}{i_0}. \quad (8)$$

Therefore, the new coefficient of losses a_1 is shown in Equation (9).

$$a_1 = U_e + U_i \frac{(T_w - T_{int})}{(T_w - T_{ext})}. \quad (9)$$

The expression of this new coefficient of losses a_1 shows that all the previous discussions about the impact of air chambers, low-emissivity coatings, and PVB layers are still valid for reducing U_e. Thus, the following subsections aim to analyze the parameters to help reduce the thermal transmittance U_i. The main goal of a solar collector is to raise the temperature of the fluid that circulates through it. However, in transparent WFG without opaque thermal insulation, there is a considerable thermal load towards the inside, given by $U_i(T_w - T_{int})$. In winter, it supplies valuable heating energy, although it worsens the glazing operation as a solar collector. In summer, the temperature difference between the fluid and indoors might negatively impact the indoor temperature. Adding an air chamber on the inside can improve the efficiency of WFG as a solar collector by reducing the thermal transmittance value to the interior, U_i. Table 5 compares thermal performance as a solar collector and transparent envelope of WFG. It shows the results of the optical efficiency of the collector, η_0, and the coefficient of thermal losses, a_1, for some glazing configurations and different tilts. The coefficient of thermal losses U_i is considerably reduced compared to cases with a single camera. The system's performance as transparent glazing is defined in this table by the g-factor visible transmittance, τ_v, which decreases as η_0 increases, as expected. Both air chambers have a low-emissivity coating on one of the surfaces, ε_2 = 0.03, and laminated glass with 07AH PVB interface.

Table 5. Comparison of thermal performance of transparent WFG as a solar collector for different tilts (horizontal $\theta = 0°$; vertical $\theta = 90°$).

Glazing	Tilt	η_0	a_1 (W/m^{2}K)	U_i (W/m^{2}K)	U_e (W/m^{2}K)	τ_v	g
4 | Air/4+4/Water/4+4 [1]	$\theta = 0°$	0.648	9.51	4.70	4.02	0.225	0.143
	$\theta = 90°$	0.647	7.83	4.72	2.33	0.225	0.143
4 | Air/4+4/Water/4+4 | Air/4 [1]	$\theta = 0°$	0.664	5.48	1.25	4.02	0.202	0.125
	$\theta = 90°$	0.661	4.13	1.54	2.33	0.202	0.125

[1] The vertical line \| defines a low emissivity coating on the air chamber surface.

The results show that the performance improves by including a second air chamber. The last WFG configuration on Table 5 is composed of two air chambers and a PVB 07AH interlayer. It has an optical efficiency η_0 = 0.661 in a vertical position, while standard plate collectors present values of 0.77. The coefficient of losses, a_1 for this WFG is 4.13 when vacuum-pipe collectors have values of 1.5 and plate collectors show values of 3.5. The panel's tilt influences the glazing's final performance, but not as much as the low-emissivity layer treatments on the closed cavities. When these coatings are applied, the coefficient of losses a_1 is reduced almost by half.

3.3. Description of a Case Study

The case study was a west-oriented curtain wall on a commercial building in Castilla La Mancha, Spain (latitude 40°04′18″ N, longitude 2°08′06″ O, altitude 920 MASL). The west-oriented WFG panels were exposed to heavy solar radiation in summer, during the afternoons. Real data from the 160 m^2 active curtain wall were collected to test the technology. The curtain wall glass was triple Water Flow Glazing (4 | /Air/4+4/Water/4+4) with 003H PVB layers with sixteen independent rows of 10 m^2. The outdoor conditions in winter are prone to freezing issues, so the fluid circulating through the WFG panels is a mixture of water and glycol. Each row includes a circulating device with a water pump and a plate heat exchanger to transfer the heat captured by the windows to a 1000 m^3 buffer tank. Figure 4 illustrates the functional layout of the facility. The temperature sensors were installed at the inlet and outlet pipes of the circulating device. One-wire probes sent data to the Electronic Control Unit in the mechanical room, where the software processed the calculations and elaborated the graphics. Flux meters were connected to the circulation pump to maintain the mass flow rate through all the modules.

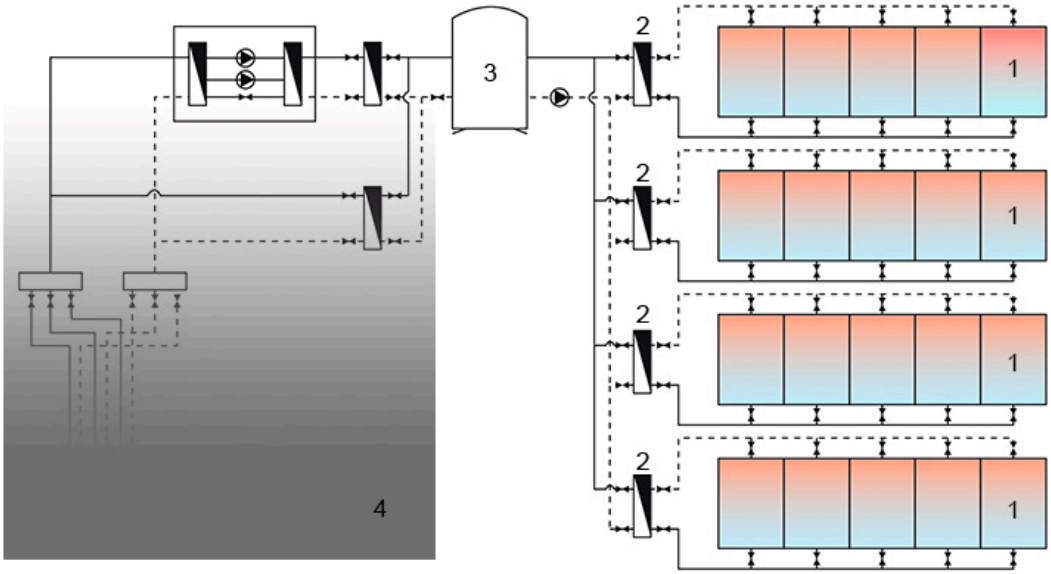

Figure 4. Schematic view of the facility's energy management system. 1. Water Flow Glazing; 2. Circulating device with the water pump and the heat exchanger; 3. Buffer tank; 4. Ground source heat pump with borehole heat exchangers.

Figure 5 shows the difference between the inlet and outlet temperatures measured the heat absorbed by these active windows. It also shows the factors that might affect the performance of a building-integrated solar collector, such as the outdoor temperature, the wind velocity, and the solar radiation on the west facade. The 12-h operation schedule from 8 am to 8 pm was evident in the sudden drop of the inlet temperature, T_{w_i}, in the morning and the rise of the same temperature in the evening. The main factors that affected the water heat absorption were the outdoor temperature and the solar radiation that showed their peak values at the maximum gap between inlet and outlet water temperatures. The wind velocity showed an average value of 3.6 m/s with peaks of 21 m/s on 9 July. The maximum temperature gap between the inlet and outlet was 9 °C when solar radiation impinged the west facade. The system schedule operated from 8:00 a.m. to 8:00 p.m. while the fluid did not circulate for the rest of the day. The maximum outdoor temperature during the three studied days was 41 °C.

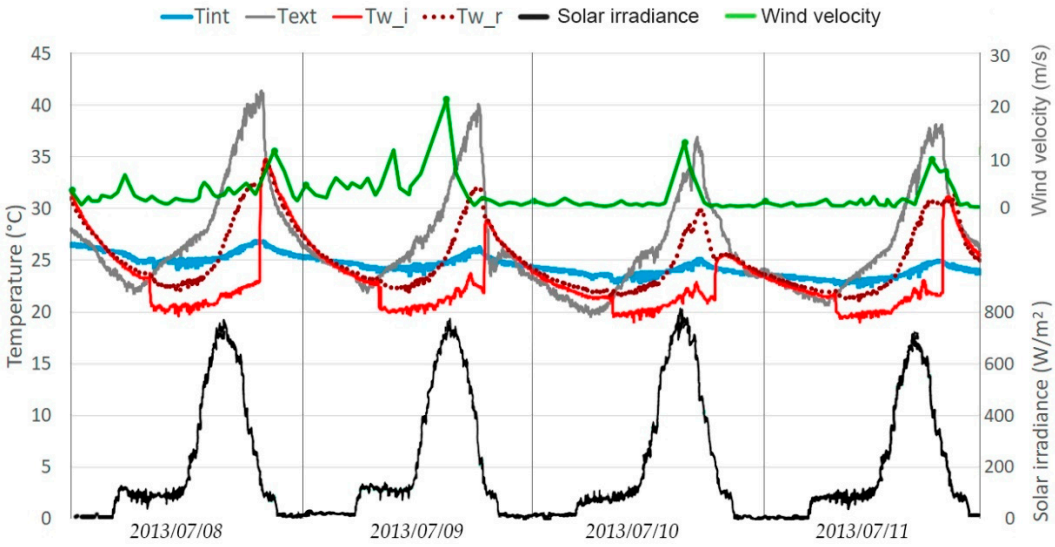

Figure 5. Daily performance of WFG in the facility on four days of July.

The inlet temperature, T_{w_i}, dropped from 24 °C to 20 °C at 8:00 a.m., when the system started operating. T_{w_r} remained above T_{w_i} until 8:00 p.m. The temperature difference between the inlet and outlet remained constant until 1:00 p.m. when the solar radiation reached the west elevation. In July, the maximum temperature difference between the inlet (T_{w_i}) and outlet (T_{w_r}) temperatures occurred at 7:15 p.m. when the solar radiation reached its peak value on the west façade. The indoor temperature graphic indicates that the transparent Water Flow Glazing curtain wall did not have a summer overheating problem, which is usually an issue in transparent curtain wall designs for passive heating. Nevertheless, indoor thermal conditions can be improved because of the ability of the WFG curtain wall to absorb part of the indoor heating loads. Figure 6 illustrates the evolution of temperatures on four days of September when the outdoor temperatures are milder, and there are fewer hours of solar radiation on the west facade.

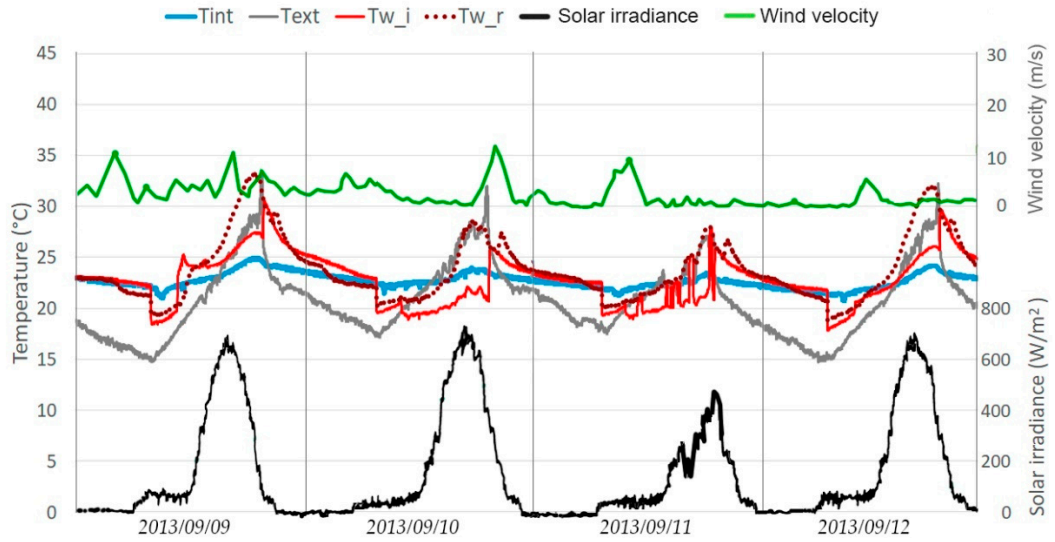

Figure 6. Daily performance of WFG in the facility on four days of September.

On clear days with a steady pattern of solar radiation, there was no water heat gain from 8:00 a.m. to 11:00 a.m. because the outdoor temperature was below 25 °C and the lack of solar radiation in the morning. After that, the temperature difference kept increasing until a peak value of 6 °C at 7:00 p.m. On 11 September, the solar radiation showed a typical pattern of a cloudy day with a lower average temperature of 18 °C. The gap

between inlet and outlet temperatures showed different values on that day. When the ambient temperature ranged between 15 °C and 29 °C, and the peak solar radiation was above 600 W/m^2, the water heat gain showed greater values.

4. Discussion

Based on the results of previous sections, a method to assess the efficiency of Water Flow Glazing as a solar collector has been validated. The following subsections develop the methodology to understand the performance under transient conditions and discuss actual data from the tested facility. Finally, economic parameters will be studied to compare the cost of traditional curtain walls and solar collectors with building-integrated Water Flow Glazing.

4.1. Nonlinear Performance in Transient Conditions

In previous sections, the efficiency parameters of WFG as solar collectors, such as η_0 and a_1, have been considered constant. Those parameters have been calculated for given temperatures, T_w = 60 °C, T_{ext} = 30 °C, and T_{int} = 25 °C. This hypothesis can lead to errors because heat transfer due to convection and radiation depends on those temperatures. The convection coefficients, h, and thermal transmittances U_i, U_e change in transient conditions. This section aims to show the nonlinear behavior of the WFG as solar collectors. The efficiency of a specific configuration will be calculated for a series of values of the reduced temperature $T_{m,e}$ by varying the outdoor temperature, T_{ext}, and considering a constant fluid temperature T_w at 60 °C, and a constant indoor interior temperature, T_{int} at 25 °C. It is challenging to know the efficiency values of the WFG in transient conditions since many parameters are involved in optical and thermal problems. Equations (8) and (9) showed an expression for the solar collector efficiency η and the coefficient of losses a_1, respectively. In transient conditions, both η and a_1 depend on the outdoor temperature when the U_i effect is included for losses. In Equation (9), the fraction that multiplies the factor U_i is variable with the outdoor temperature T_{ext}. As T_{ext} decreases, the contribution of U_i to the coefficient a_1 is lower. Table 6 shows some discrete values used to calculate the efficiency, according to Equations (8) and (9), with an external solar irradiance of 800 W/m^2. Column η (facade) shows the efficiency for the best transparent WFG configuration presented in previous sections, triple WFG (4 | Air/4++4/Water/4++4 |) in a vertical position, with a double interlayer of PVB 003H and low-emissivity coating on the inner face. Column η (collector) shows the efficiency when opaque thermal insulation has been placed on the inner face of the WFG with the hypothesis of U_i = 0. The same triple WFG has been used except for the lack of low-emissivity coating on the inner side.

Table 6. Comparison of thermal performance as a solar collector $\eta_{(collector)}$ and transparent envelope $\eta_{(facade)}$ of WFG for different outdoor temperatures.

$T_{m,e}$ (m^{2}K/W)	T_{ext} (°C)	η_0	a_1 (W/m^{2}K)	U_e (W/m^{2}K)	[1] U_i (W/m^{2}K)	$\eta_{(facade)}$	$\eta_{(collector)}$
0.000	60	0.738	-	1.85	0.25/0	0.727	0.738
0.001	59	0.738	10.59	1.84	0.25/0	0.725	0.736
0.006	55	0.738	3.58	1.83	0.25/0	0.716	0.727
0.013	50	0.738	2.71	1.83	0.25/0	0.704	0.715
0.025	40	0.738	2.40	1.97	0.25/0	0.678	0.689
0.038	30	0.738	2.64	2.35	0.25/0	0.639	0.650
0.050	20	0.739	3.06	2.84	0.25/0	0.586	0.597
0.063	10	0.740	3.26	3.08	0.25/0	0.537	0.547
0.075	0	0.740	3.44	3.30	0.25/0	0.482	0.493
0.088	−20	0.741	3.62	3.50	0.25/0	0.424	0.435
0.100	−30	0.742	3.80	3.69	0.25/0	0.362	0.373

[1] U_i = 0 when opaque with thermal insulation on the inner face of the WFG (collector).

Figure 7 compares the efficiency of triple WFG (4|Air/4++4/Water/4++4|) with conventional solar collectors available in the market. Two options have been considered for the WFG. The first one is a solar collector with opaque thermal insulation and the second one is a transparent envelope. Both WFG case studies have a low emissivity coating in the air chamber. The solar irradiance has been fixed at 800 W/m^2, whereas the outdoor temperature varies.

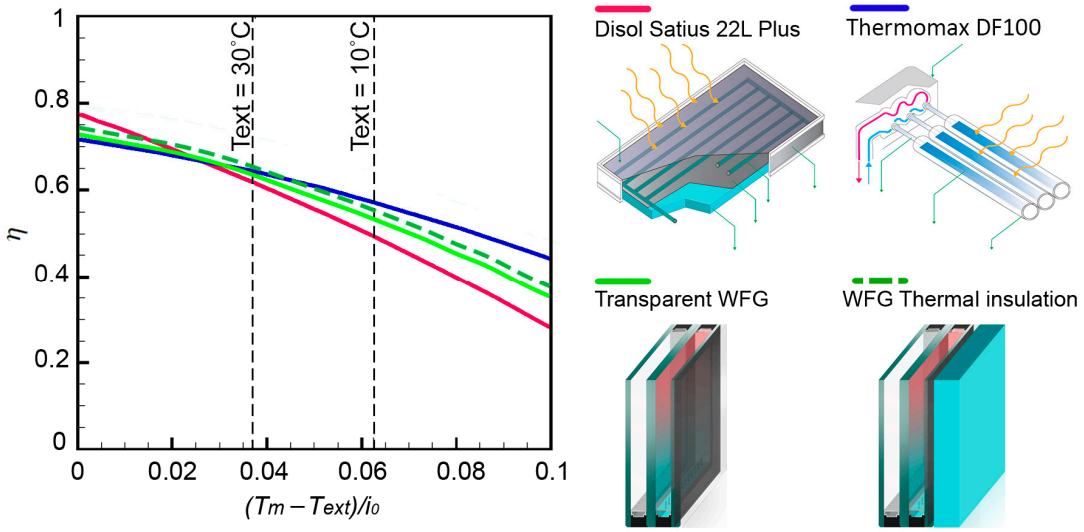

Figure 7. Water Flow Glazing as solar collector efficiency compared to commercial flat-plate and vacuum-pipe collectors.

4.2. Tested Facility

Section 3.3 showed the ability of a transparent WFG curtain wall to heat up the water in an actual building. The current section discussed the data and the total energy absorbed by water in the 160 m^2 curtain wall. Afterward, that energy was compared with the needs of domestic hot water of the analyzed facility, according to the Spanish code DB-CTE-HE4 [40]. The f-chart method, developed by S.A. Klein, W.A. Beckman, and J.A. Duffie in 1976, estimates the annual thermal performance of active heating systems for buildings [41]. Some authors have shown a good relationship between empirical data and the f-chart projections [42]. Three variables affect the f-chart results: the first variable is the collector area; the second one is the collector type defined by its performance; the third one is defined by the storage capacity, fluid flow rates, and heat exchangers. The fraction of the monthly demand supplied by the collectors, f, is a function of two dimensionless variables; X: ratio of collector losses to heating loads and Y: ratio of absorbed solar radiation to heating loads. The f-chart method requires two values to describe the solar collector: the optical efficiency and the coefficient of losses. According to Table 5, for the selected triple Water Flow Glazing (4|/Air/4+4/Water/4+4), the optical efficiency was 0.647, and the coefficient of losses was 7.83. The f value was calculated monthly and annually with an average consumption of 2000 L per day. Table 7 summarizes the results. Where $T_{w\,supply}$ is the temperature of the water supply, $Gd_i(0)$ is the solar radiation on a horizontal surface for the selected site, *DE* is the monthly demand for Domestic Hot Water, *EI* is the solar radiation impinging on the glazing, and *EU* is the total energy delivered by the solar collectors. The input data was taken from the Spanish code for solar thermal systems [43]. In January, the WFG curtain wall could deliver 35% of the requested thermal energy. The highest thermal energy supplied by the system was in September, with 87% of domestic hot water demand. The fraction of the annual domestic hot water demand provided by solar energy was 60%, the fraction requested by the document DB CTE HE4.

Table 7. Results of the WFG curtain wall with the f-chart method.

Month	T_{ext} (°C)	$T_{w\ supply}$ (°C)	$Gd_i(0)$ (kWh/m^2 day)	DE (kWh)	EI (kWh/m^2)	EU (kWh)	f
January	5	4	1.64	4027	41.50	1437	0.357
February	6	5	2.44	3572	46.59	1766	0.494
March	9	7	3.58	3811	58.10	2223	0.583
April	12	9	4.83	3549	51.95	1927	0.543
May	15	10	5.19	3596	40.38	1355	0.377
June	20	11	6.11	3410	38.09	1347	0.395
July	24	12	7.11	3453	53.70	2153	0.624
August	23	11	6.19	3524	68.79	2761	0.784
September	20	10	4.86	3480	79.41	3033	0.872
October	14	9	3.11	3667	73.94	2809	0.766
November	9	7	2.00	3688	55.46	2188	0.574
December	6	4	1.53	4027	43.78	1600	0.398
Average	13.5	8.25		3651	54.31	2044	0.605

Equation (10) shows the expression of the water heat gain, P in Water Flow Glazing panels [24].

$$P = \dot{m}c(T_{w\_r} - T_{w\_i}), \tag{10}$$

where T_{w_i} is the temperature of the water inlet entering the glazing and T_{w_r} is the temperature of the water returning to the circulating device; $\dot{m}$ is the mass flow rate, and c is the specific heat of the fluid. The mass flow rate was set to 0.9 (L/min m^2) and the fluid's specific heat was 2800 (J/kg K). Figure 8 summarizes the water heat gains on four sample days in July and September. The average daily absorption in July was 205 kWh. The WFG curtain wall showed a daily average absorption of 168 kWh in September with a maximum temperature difference between the inlet and outlet from 5:00 p.m. to 7:00 p.m. As it was shown in Figure 6, solar radiation on the west facade showed high values in the west facade, with a peak solar radiation of 680 (W/m^2) at 5:00 p.m.

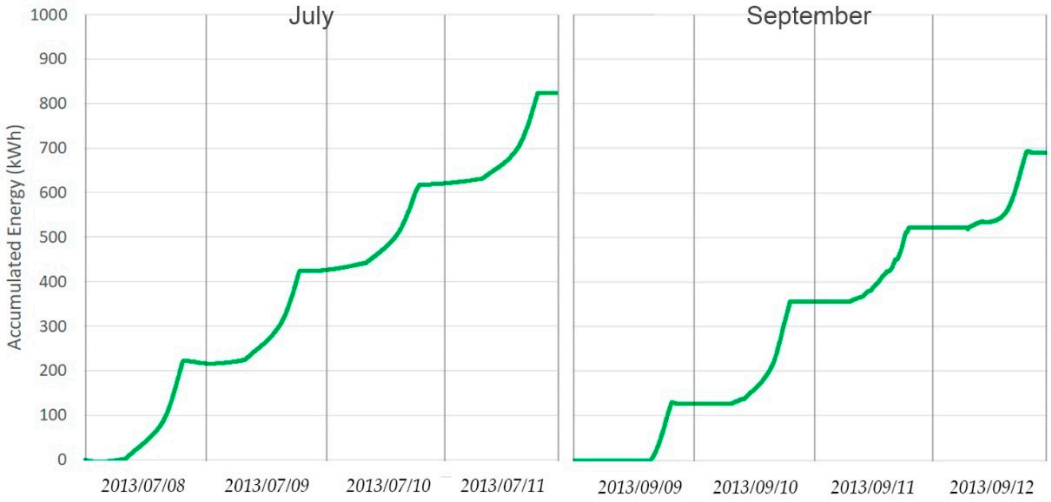

Figure 8. Accumulated energy in the curtain wall on four days of July and September.

Researchers at the Polytechnic University of Madrid published in scientific journals a methodology to estimate the energy behavior of Water Flow Glazing curtain walls under transient conditions [23,26]. The contribution of this paper was to explore and validate that methodology to assess the ability of Water Flow glazing to produce hot water as a building-integrated solar collector. Equation (11) shows the expression of the outlet water temperature of a WFG panel (T_{w_r}) as a function of transient parameters, such as the inlet temperature (T_{w_i}), and indoor and outdoor temperatures, (T_{int}) and (T_{ext}). The rest of the

parameters were considered steady: the mass flow rate, $\dot{m}$, the specific heat of the fluid, c, and the heat transfer coefficients, U_e and U_i. The convective heat transfer coefficients were considered constant values, according to other scientific articles [18,33]. Therefore, the constant value for h_i was 8 W/m^{2}K, h_e was 23 W/m^{2}K, the heat transfer coefficient of the water chamber, h_w, was 50 W/m^{2}K, the heat transfer coefficient of the air cavity was h_g = 5.3 W/m^{2}K, and finally, the specific heat capacity of the fluid, c was 2800 J/kg K.

$$T_{w\_r} = \frac{i_0 A_v + U_i T_{int} + U_e T_{ext} + \dot{m} c T_{w\_i}}{\dot{m} c + U_e + U_i}. \tag{11}$$

where A_v is the absorptance of the WFG panel. Equation (12) shows the absorptance, A_v, that depends on the energy absorbed by the glass panes and by the water:

$$A_v = A_1 \left(\frac{U_e}{h_e} \right) + A_2 \left(\frac{1}{h_g} + \frac{1}{h_e} \right) U_e + A_3 \left(\frac{U_i}{h_i} \right) + A_w. \tag{12}$$

where A_1 is the absorptance of the exterior glass pane, A_2, is the absorptance of the middle glass pane, and A_3 are the absorptance of the interior one. A_w is the absorptance of the water chamber. The convective coefficients were defined before, whereas U_e and U_i were calculated with Equations (4) and (5). Table 8 shows the absorptances of the WFG panel used in the case study that were taken from previous articles [33].

Table 8. Absorptances of the glass panes and water chamber.

	A_1	A_2	A_3	A_w	A_v
WFG	0.04	0.25	0.06	0.15	0.27

Equation (13) results from replacing the values of T_{w_r} in Equation (10).

$$P = \frac{\dot{m} c}{\dot{m} c + U_e + U_i} (i_0 A_v + U_i (T_{int} - T_{w\_i}) + U_e (T_{ext} - T_{w\_i})). \tag{13}$$

To simulate transient conditions, the weather file EPW (EnergyPlus Weather Office of Energy Efficiency & Renewable Energy, Washington, DC, USA) for Cuenca, Spain, was considered for the outdoor temperature and solar irradiance. The indoor temperature (T_{int}) and inlet temperature (T_{w_i}) were considered constant boundary conditions in the simulation, and heat transfer coefficients remained constant to avoid uncertainties in the validation process. Regarding the mass flow rate, it was a constant value of 0.9 (L/min m^2). Figure 9 illustrates the difference between actual and simulated results for accumulated energy on 7 July and 10 September. The water heat gain was measured by the difference between inlet and outlet temperatures, and the simulated results were calculated using Equation (13). The indoor temperature for the simulation was 25 °C in July and 23 °C in September, whereas the inlet temperature was 20 °C in both cases. The figure illustrates that the measured values for indoor and inlet temperature were close to the considered values for the simulation over the working period of the facility, from 8:00 a.m. to 8:00 p.m.

Root Mean Square Error (RMSE) and the Normalized Root Mean Square Error (NRMSE), shown in Equations (14) and (15), were used to validate the simulation results against the actual measured values. ASHRAE Guideline 14-2014 suggests the use of a normalization means, nm to verify the accuracy of the simulation [44].

$$RMSE = \sqrt{\frac{\sum_{i=1}^{n} |E_{Si} - E_{Ri}|}{n}}, \tag{14}$$

$$NRMSE = \frac{1}{nm} \sqrt{\frac{\sum_{i=1}^{n} |E_{Si} - E_{Ri}|}{n}} \, 100, \tag{15}$$

where E_{Si} is the simulated value for accumulated energy, E_{Ri} is the measured value, and nm is defined in Equation (16) as per ASHRAE recommendations, as the average of measured values, E_{Ri}

$$nm = \frac{\sum_{i=1}^{n} E_{Ri}}{n}. \quad (16)$$

RMSE and NRMSE were calculated with a total number of measurements, n of 1442 on each day. The RMSE was 10.6 and the NRMSE was 14.5%. As per ASHRAE Guideline 14, a NRMSE below 25% indicates a good model fit with acceptable predictive capabilities. For the considered dataset of values taken every 5 min on 7 July and 10 September given above, NRMSE was found to be 14.5%, implying that the model is reliable.

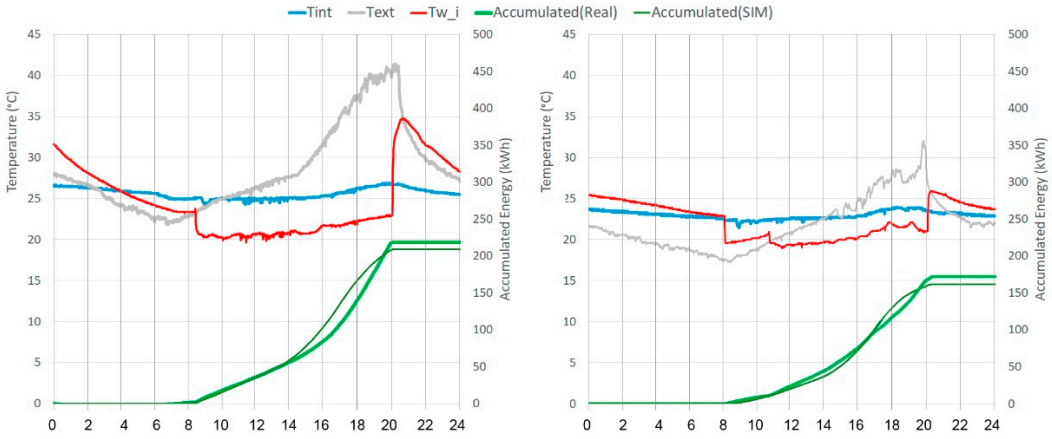

Figure 9. Comparison of simulated and measured accumulated energy on two days of July and September.

4.3. Cost Comparison

The values of the total energy delivered by the solar collectors, *EU*, from Table 7 were compared with the values from actual data in September. The same f-chart method was used to compare the performance of WFG as a solar collector with 30 m^2 south oriented with a tilt of 45° of Disol Satius 22 L Plus with an optical efficiency of 0.775 and a coefficient of losses of 3.73. The hot water consumption was 2000 L per day. Table 9 illustrates that this solar collector system covered 60% of hot water demand.

Table 9. Results of the Disol Satius 22 L Plus solar collector system with the f-chart method.

Month	T_{ext} (°C)	$T_{w\ supply}$ (°C)	$Gd_i(0)$ (kWh/m^2 day)	*DE* (kWh)	*EI* (kWh/m^2)	*EU* (kWh)	*f*
January	5	4	1.64	4027	71.13	1160	0.288
February	6	5	2.44	3572	88.29	1468	0.411
March	9	7	3.58	3811	127.75	2098	0.550
April	12	9	4.83	3549	146.45	2343	0.660
May	15	10	5.19	3596	146.54	2353	0.654
June	20	11	6.11	3410	161.33	2551	0.748
July	24	12	7.11	3453	202.81	3068	0.889
August	23	11	6.19	3524	197.79	3038	0.862
September	20	10	4.86	3480	175.00	2752	0.791
October	14	9	3.11	3667	134.06	2188	0.597
November	9	7	2.00	3688	91.20	1504	0.408
December	6	4	1.53	4027	71.04	1166	0.290
Average	13.5	8.25		3651	134.45	1160	0.601

The water-energy absorption can be used as renewable primary energy production, whereas the heat absorbed by the water does not affect the cooling loads inside the building.

The optimum Water Flow Glazing to work as a solar collector requires triple glazing with an air chamber with a low-emissivity coating and a dark PVB interlayer. Section 4.1 has shown that optical efficiencies and thermal loss coefficients are similar to those of commercial plate collectors shown in Table 1. Therefore, it is necessary to assess the economic parameters of both systems to understand the viability of Water Flow Glazing as an integrated system to produce renewable energy in buildings. Table 10 compares the market price of commercial solar collectors with the price per square meter of the WFG. Vacuum pipe collectors are more pricy than solar plate collectors, as they use more advanced technology and are prepared to perform well in adverse conditions. However, triple WFG with optical efficiency η_0 of 0.647 and coefficient of losses a_1 of 7.83 has a competitive price per square meter compared with other solar collectors. In addition, it allows building designers to choose the glazing surface, thus adapting to the client's needs in each case. The cost of commercial thermal collectors came from the ITeC database [45].

Table 10. The cost of solar collectors compared to the cost of a Triple WFG 4 | Air/4++4/Water/4++4 with low-emissive coating in the air chamber and PVB 003H.

Collector Type	Model	Price (€)	Area (m^2)	(€/m^2)
Flat plate	Disol Satius 22 L Plus [1]	713	1.97	362
Vacuum-pipe	Thermomax DF100 [1]	972	1.92	506
WFG	4 | Aire/4++4/Agua/4++4	-	Defined by user	370

[1] Costs of commercial solar collectors were taken from [45].

The perfect case study for building-integrated water flow glazing would be a high-rise office building with limited roof area and a repetitive facade geometry easily divided in panels with no need of movable windows. The cost analysis compared two unitized façades considering a triple glass, aluminum production, module fabrication, on-site transportation, and facade assembly. These values are the average unit costs of two passive curtain wall systems [46–48]. WFG costs included a triple glass (4 | Air/4++4/Water/4++4 |) with a double interlayer of PVB 003H and low-emissivity coating on the inner face, a special unitized frame, and finally a circulating system. Table 11 illustrates the construction costs calculated for all the alternatives.

Table 11. The cost of the curtain wall with a Triple WFG compared with the reference building with traditional curtain wall and commercial solar collectors.

Case Study	Glass (€/m^2)	Aluminum Frame (€/m^2)	Circulating Device (€/m^2)	Solar Collectors (€/m^2)	Total (€)
WFG [1]	370	415	150	-	149,600
Reference Building [1]	220	415	-	362	112,460

[1] Costs for the Reference Building were taken from [24]. WFG components were taken from [45].

As stated in Section 4.2, the area of the curtain wall was 160 m^2 whereas the area of the solar collectors Disol Satius 22 L Plus was 30 m^2 for the same delivered energy.

5. Conclusions

The chapter's primary goal has been to study the adequate performance of Water Flow Glazing as solar thermal collectors. The study of the properties of the two types of solar collectors on the market concluded that vacuum tube collectors, although more expensive, perform better on sunny days or when the weather conditions are extreme.

The efficiency of commercial solar collectors depends on two properties: optical efficiency and the coefficient of losses. Section 2 developed a method to assess the efficiency of Water Flow Glazing panels as water-heating devices. As a result, a thermal transmittance to the interior, U_i, appeared in WFG when it did not have any thermal insulation on the

interior face. By placing opaque thermal insulation on the inner face of the WFG, the value of U_i was zero. Triple WFG with thermal insulation with dark butyral interlayers between two glass panes and low-emissive coatings improves the system's performance with an optical efficiency of 0.765 and a coefficient of losses of 3.40. Those values are similar to flat plate collectors with an optical efficiency of 0.792 and a coefficient of losses of 3.67. Transparent triple WFG with dark butyral interlayers between two glass panes and low-emissive coatings yielded optical efficiencies of 0.648, and a coefficient of losses of 9.51, whereas the visible transmittance was 0.225.

Transparent WFG is necessary when placed on curtain walls, so architects might discard the hypothesis of $U_i = 0$ for building integrated solar collectors. Section 4 discussed the performance of transparent WFG in a real case study. The total energy delivered by the active 160 m^2 curtain wall with a west orientation was similar to the energy produced by 30 m^2 south-oriented flat plate collectors with a tilt of 45. Finally, Section 4.3 compared the costs of both solutions. The final price of the WFG curtain wall was 33% higher than a reference building with a traditional curtain wall and flat plate solar collectors.

Several factors affect solar panels and generate uncertainty in efficiency and performance. Outdoor solar radiation and temperature, along with wind velocity, are usually considered to assess the efficiency of traditional solar collectors. In addition, other factors, like solar obstructions or the dust accumulated in the panel, can change the expected outcomes of the collector. Using building-integrated solar collectors can improve the integration of renewable energies in facades and roofs but also increase the factors that affect their efficiency. These collectors can be in contact with indoor air, so specific parameters of indoor air quality, such as the ventilation, rate, occupant's activities, internal heat loads, and heating and cooling systems in general, end up affecting the solar collector's efficiency. Moreover, transparent collectors with warm water running through them can cause overheating inside the building. Future research needs to address these uncertainties by measuring test prototypes and existing facilities to make the simulation models more consistent. Water Flow Glazing must address some challenges as building-integrated solar collectors. Firstly, an advanced energy management system with meters and actuators is necessary to assess the ability to produce warm water and to reduce heating and cooling loads in the building. Secondly, real case studies in different climates must be analyzed. Finally, a whole commissioning protocol must include design, manufacturing, and maintenance to involve construction stakeholders in adopting new products. The initial prices of the WFG, made up of the triple glazing, the circulating device, and the unitized aluminum frames, are high compared to traditional curtain walls. However, a holistic approach should include a life cycle analysis of energy savings, on-site renewable energy production, and CO_2 emissions.

Author Contributions: Conceptualization, F.d.A.G. and J.A.H.R.; methodology, J.A.H.R.; software, J.A.H.R.; validation, B.M.S. and F.d.A.G.; formal analysis, B.M.S. and F.d.A.G.; investigation, F.d.A.G.; resources, B.M.S.; data curation, F.d.A.G. and J.A.H.R.; writing—original draft preparation, F.d.A.G. and J.A.H.R.; writing—review and editing, B.M.S.; visualization, F.d.A.G.; supervision, J.A.H.R.; funding acquisition, F.d.A.G. All authors have read and agreed to the published version of the manuscript.

Funding: This research received no external funding.

Institutional Review Board Statement: Not applicable. The review did not involve any humans or animals.

Data Availability Statement: Not applicable.

Acknowledgments: This work was supported by Keene State College Faculty Development Grant program.

Conflicts of Interest: The authors declare no conflict of interest.

Appendix A

The Appendix includes information about the commercial solar collectors used as a reference for this article.

FICHA TÉCNICA CAPTADOR SOLAR DISOL SATIUS 22L PLUS

- Captador solar plano certificado de alta eficiencia.
- Absorbedor de cobre con recubrimiento altamente selectivo de óxido de titanio y soldadura láser.
- Circuito absorbedor de cobre tipo serpentín.
- Cubierta de vidrio templado de 3.2 mm de espesor y bajo contenido en hierro.
- Marco de aluminio provisto de mecanización especial para fijación a la estructura soporte.
- Acoplamiento para sonda de temperatura en contacto con el absorbedor que asegura un óptimo control de la temperatura del captador, sin necesidad de elementos o accesorios externos.
- Aislamiento de lana mineral de elevado espesor: 50 mm.
- Interconexión mediante racores bicono.
- Accesorios de conexión incluidos en el kit de estructura.
- Instalación en posición vertical.
- Excelentes costes de montaje en instalaciones de cualquier tamaño.

COMPONENTES	
Absorbedor	Lámina de cobre con recubrimiento selectivo de óxido de titanio y absorbedor formado por un tubo de cobre de 9 mm en forma de serpentín unido a 2 tubos colectores de cobre de Ø 22 mm
Cubierta transparente	Vidrio solar de seguridad y bajo contenido en hierro, templado, de espesor 3,2 mm.
Caja captador	Marco de perfil de aluminio extruido. Fondo realizado en lámina de aluminio
Aislamiento térmico	Lana mineral de 50 mm de espesor
Conexiones	4 salidas laterales en tubo de cobre de 22
Características constructivas y dimensionales	
Dimensiones externas (mm)	1870 x 1150 x 95 (2.18 m²)
Dimensiones absorbedor (mm)	1.97
Dimensiones apertura (mm)	1.97
Peso en vacío (kg)	34
Capacidad de líquido (l)	1.7
Características funcionales	
Presión máxima de trabajo (bar)	10
Temperatura de estancamiento (ºC)	217º
Fluido de trabajo	Agua o agua + anticongelante
ABSORTIVIDAD Y EMISIVIDAD	95% - 5%
CURVA DE RENDIMIENTO $\eta = \eta_0 - a_1 (\Delta T/G) - a_2 \Delta T^2/G$ Referente al área de apertura	η_0: 0,775 Coeficiente de pérdidas a_1: 3.73 W/(m²K) Coeficiente de pérdidas a_2:0.0152 W/(m²K²) Contraseña Certificación: NPS-13708

©DISOL FTCS_SATIUS 22L PLUS_v0901 FICHA TÉCNICA CAPTADOR SOLAR SATIUS 22L PLUS

After over 25 years of manufacturing and development, Thermomax evacuated tube collectors are firmly established as a world leader in solar thermal products.

Easy Installation

The unique 'plug and play' design of Thermomax solar collectors makes installation quick and easy. There is no need for heavy lifting equipment as tubes can be carried onto the roof individually. The collector is fixed to the roof by easy-fit brackets, which are simply fixed to the rafter.

Performance and Savings

- Designed specifically for Northern European climates, Thermomax products provide heat even in cold, windy or humid conditions
- A superior vacuum in the tube, over a longer period of time
- Supplies up to 70% of your annual hot water needs - reducing dependence on increasingly expensive fossil fuels
- 5 year standard warranty. 20 year warranty with a Kingspan Solar Accredited Installer
- Works from dawn until dusk and throughout the year
- 30% more effective than flat plate collectors
- Average 25-year lifespan

DF100 is a direct flow solar collector, which consists of a row of solar tubes and a highly insulated manifold. The heat medium to be heated is passed down through the collector tube within a coaxial heat exchanger.

The vacuum inside each tube provides perfect insulation and therefore protects the system from outside influences such as cold and windy weather or high humidity. This vacuum insulation also ensures that the energy collected from the sun is very efficiently and effectively transferred into usable heat

Chose DF100 for versatility

DF100 can be installed on a pitched or horizontal surface, and the tube can be rotated 25° to compensate for installations that deviate from south. As the collector is a fully pumped unit, there is no minimum angle for the collector.

Installation Options

Collector Positions
1 Ideal slope 40°
2 Roof kit angled 40°
3 Elevated 20°
4 Horizontal ideal slope
5 Horizontal façade
6 Flat
7 Vertical façade

DF100 collectors are available in 3 different sizes

	DF100		
	1mY	2mY	3mY
Number of Tubes	10	20	30
Dimensions			
Absorber Area (m²)	1.002	2.004	3.020
Overall Dimensions (mm)	1996 x 709 x 97	1996 x 1488 x 97	1996 x 2827 x 97
Width of Manifold (mm)	709	1488	2127
Length (tube and manifold) (mm)	1996	1996	1996
Depth (mm)	97	97	97
Aperture Area (m²)	107	215	323
Fluid Volume (ltr)	1.8	3.6	5.6
Inlet and Outlet Dimensions (mm)	22	22	22
Weight (empty) (kg)	25	54.8	84.4
Mounting			
Recommended Inclination (°)	0-90	0-90	0-90
Performance Data			
Efficiency	Based on Aperture	Based on Aperture	Based on Aperture
Eta0	0.781	0.773	0.779
a1 (W/m²K)	1.44	1.43	1.07
a2 (W/m²K²)	0.0062	0.0059	0.0815
Solar Keymark Licence Numbers	011-7S060R	011-7S060R	011-7S060R
Operating Data			
Flow Rate (ltr/h)			
Rated	80	160	240
Minimum	60	120	180
Maximum	150	300	480
Maximum Operating Pressure	8 Bar	8 Bar	8 Bar
Stagnation Temperature (°C)	286	286	286
Heat Transfer Fluid	Water / Glycol	Water / Glycol	Water / Glycol
Materials			
Absorber Coating	Copper Selective Coating	Copper Selective Coating	Copper Selective Coating
Absorbance (%)	95	95	95
Emissivity (%)	5	5	5
Mounting Frame and Clips	Stainless Steel, Aluminium, EPDM	Stainless Steel, Aluminium, EPDM	Stainless Steel, Aluminium, EPDM
Glass	Low Iron - Transm. 0.92	Low Iron - Transm. 0.92	Low Iron - Transm. 0.92
Vacuum	<10⁻²mbar	<10⁻²mbar	<10⁻²mbar
Quality Certification / Solar Keymark	Yes	Yes	Yes

Contact us now for further information
Tel. +44 (0) 28 3836 4500 or email us at info@kingspansolar.com

References

1. European Union. Directive (EU) 2018/844 of the European Parliament and of the Council of 30 May 2018. Amending Directive 2010/31/EU on the Energy Performance of Buildings and Directive 2012/27/EU on Energy Efficiency. 2018. Available online: https://eur-lex.europa.eu/legal-content/EN/TXT/PDF/?uri=CELEX:32018L0844&from=EN (accessed on 25 July 2022).
2. Kumar, R.; Rosen, M. A critical review of photovoltaic–thermal solar collectors for air heating. *Appl. Energy* **2011**, *88*, 3603–3614. [CrossRef]
3. Baljit, S.S.S.; Chan, H.Y.; Sopian, K. Review of building integrated applications of photovoltaic and solar thermal systems. *J. Clean. Prod.* **2016**, *137*, 677–689. [CrossRef]
4. Sami Buker, M.; Riffat, S. Building integrated solar thermal collectors—A review. *Renew. Sustain. Energy Rev.* **2015**, *51*, 327–346. [CrossRef]
5. Vassiliades, C.; Agathokleous, R.; Barone, G.; Forzano, C.; Giuzio, G.F.; Palombo, A.; Buonomano, A.; Kalogirou, S. Building integration of active solar energy systems: A review of geometrical and architectural characteristics. *Renew. Sustain. Energy Rev.* **2022**, *164*, 112482. [CrossRef]
6. Moskwa-Bęczkowska, D.; Moskwa, A. Renewable Energy Sources in the Processes of Thermal Modernization of Buildings—Selected Aspects in Poland. *Energies* **2022**, *15*, 4613. [CrossRef]
7. Vassiliades, C.; Kalogirou, S.; Michael, A.; Savvides, A. A roadmap for the integration of active solar systems into buildings. *Appl. Sci.* **2019**, *9*, 2462. [CrossRef]
8. Leonzio, G. Solar systems integrated with absorption heat pumps and thermal energy storages: State of art. *Renew. Sustain. Energy Rev.* **2017**, *70*, 492–505. [CrossRef]
9. Ravi Kumar, K.; Krishna Chaitanya, N.V.V.; Sendhil Kumar, N. Solar thermal energy technologies and its applications for process heating and power generation—A review. *J. Clean. Prod.* **2021**, *282*, 125296. [CrossRef]
10. Rybár, R.; Beer, M.; Mudarri, T.; Zhironkin, S.; Bačová, K.; Dugas, J. Experimental Evaluation of an Innovative Non-Metallic Flat Plate Solar Collector. *Energies* **2021**, *14*, 6240. [CrossRef]
11. Ider, J.; Oliveira, A.; Rubinger, R.; Silva, A.K.; Assini, A.; Tiago-Filho, G.; Baldissera, M. Concentrated Solar Power with Thermoelectric Generator—An Approach Using the Cross-Entropy Optimization Method. *Energies* **2022**, *15*, 4774. [CrossRef]
12. Papadimitratos, A.; Sobhansarbandi, S.; Pozdin, V.; Zakhidov, A.; Hassanipour, F. Evacuated tube solar collectors integrated with phase change materials. *Sol. Energy* **2016**, *129*, 10–19. [CrossRef]
13. Zhu, C.; Dong, X.; Yan, S.; Cui, Y.; Luo, Q. Air-Type Vacuum-Tube Solar Collector Design and Heat Collection Performance Test. *Energies* **2022**, *15*, 5679. [CrossRef]

14. Popsueva, V.; Lopez, A.F.O.; Kosinska, A.; Nikolaev, O.; Balakin, B.V. Field Study on the Thermal Performance of Vacuum Tube Solar Collectors in the Climate Conditions of Western Norway. *Energies* **2021**, *14*, 2745. [CrossRef]
15. Tomas, M.; Borivoj, S. Facade solar collectors. *Sol. Energy* **2006**, *80*, 1443–1452.
16. Rockendorf, G.; Janssen, S.; Felten, H. Transparently insulated hybrid wall. *Sol. Energy* **1996**, *58*, 33–38. [CrossRef]
17. Chow, T.T.; Li, C.; Lin, Z. The function of solar absorbing window as water-heating device. *Build. Environ.* **2011**, *46*, 955–960. [CrossRef]
18. Chow, T.T.; Li, C.; Lin, Z. Thermal characteristics of water-flow double-pane window. *Int. J. Therm. Sci.* **2010**, *50*, 140–148. [CrossRef]
19. Gil-Lopez, T.; Gimenez-Molina, C. Influence of double glazing with a circulating water chamber on the thermal energy savings in buildings. *Energy Build.* **2013**, *56*, 56–65. [CrossRef]
20. Gutai, M.; Kheybari, A.G. Energy consumption of hybrid smart water-filled glass (SWFG) building envelope. *Energy Build.* **2021**, *230*, 110508. [CrossRef]
21. Lyu, Y.L.; Chow, T.T.; Wang, J.L. Numerical prediction of thermal performance of liquid-flow window in different climates with anti-freeze. *Energy* **2018**, *157*, 412–423. [CrossRef]
22. Lyu, Y.L.; Wu, X.; Li, C.; Su, H.; He, L. Numerical analysis on the effectiveness of warm water supply in water flow window for room heating. *Sol. Energy* **2019**, *177*, 347–354. [CrossRef]
23. Moreno Santamaria, B.; Ama Gonzalo, F.; Lauret Aguirregabiria, B.; Hernandez Ramos, J.A. Evaluation of Thermal Comfort and Energy Consumption of Water Flow Glazing as a Radiant Heating and Cooling System: A Case Study of an Office Space. *Sustainability* **2020**, *12*, 7596. [CrossRef]
24. Del Ama Gonzalo, F.; Moreno Santamaria, B.; Ferrándiz Gea, J.A.; Griffin, M.; Hernandez Ramos, J.A. Zero Energy Building Economic and Energetic Assessment with Simulated and Real Data Using Photovoltaics and Water Flow Glazing. *Energies* **2021**, *14*, 3272. [CrossRef]
25. Moreno Santamaria, B.; del Ama Gonzalo, F.; Lauret Aguirregabiria, B.; Hernandez Ramos, J.A. Experimental Validation of Water Flow Glazing: Transient Response in Real Test Rooms. *Sustainability* **2020**, *12*, 5734. [CrossRef]
26. Moreno Santamaria, B.; del Ama Gonzalo, F.; Pinette, D.; Gonzalez-Lezcano, R.-A.; Lauret Aguirregabiria, B.; Hernandez Ramos, J.A. Application and Validation of a Dynamic Energy Simulation Tool: A Case Study with Water Flow Glazing Envelope. *Energies* **2020**, *13*, 3203. [CrossRef]
27. *UNE-EN 12975-2:2006*; Thermal Solar Systems and Components-Solar Collectors-Part 2: Test Methods. AENOR (Spanish Association for Standardization and Certification): Madrid, Spain, 2007.
28. Garg, H.P.; Rani, U. Loss coefficients from solar flat-plate collectors. *Appl. Energy* **1980**, *7*, 109–117. [CrossRef]
29. *ISO 9488:2022*; Solar Energy—Vocabulary. International Organization for Standardization: Geneva, Switzerland, 2022.
30. Evangelisti, L.; De Lieto, R.; Asdrubali, V.F. Latest advances on solar thermal collectors: A comprehensive review. *Renew. Sustain. Energy Rev.* **2019**, *114*, 109318. [CrossRef]
31. Harrison, S.; Cruickshank, C.A. A review of strategies for the control of high temperature stagnation in solar collectors and systems. *Energy Procedia* **2012**, *30*, 793–804. [CrossRef]
32. Resch, K.; Wallner, G.M. Thermotropic layers for flat-plate collectors—A review of various concepts for overheating protection with polymeric materials. *Sol. Energy Mater. Sol. Cells* **2009**, *93*, 119–128. [CrossRef]
33. Sierra, P.; Hernandez, J.A. Solar heat gain coefficient of water flow glazing. *Energy Build.* **2017**, *139*, 133–145. [CrossRef]
34. *ISO 15099:2003*; Thermal Performance of Windows, Doors and Shading Devices—Detailed Calculations. International Organization for Standardization: Geneva, Switzerland, 2004.
35. Karimirad, M.; Rosa-Clot, M.; Armstrong, A.; Whittaker, T. Floating solar: Beyond the state of the art technology. *Sol. Energy* **2021**, *219*, 1–2. [CrossRef]
36. Barone, G.; Buonomano, A.; Forzano, C.; Palombo, A. Building Energy Performance Analysis: An Experimental Validation of an In-House Dynamic Simulation Tool through a Real Test Room. *Energies* **2019**, *12*, 4107. [CrossRef]
37. Del Linz, P.; Hooper, P.A.; Arora, H.; Wang, Y.; Smith, D.; Blackman, B.R.K.; Dear, J.P. Delamination properties of laminated glass windows subject to blast loading. *Int. J. Impact Eng.* **2017**, *105*, 39–53. [CrossRef]
38. Vedrtnam, A.; Pawar, S.J. Laminated glass: Classification, characterization, and future perspectives. *J. Mater. Educ.* **2020**, *42*, 51–61.
39. Vanceva Technical Documents. Available online: https://www.vanceva.com/learn/technical-documents (accessed on 15 July 2022).
40. DB CTE HE4. Available online: https://www.codigotecnico.org/pdf/Documentos/HE/DBHE.pdf (accessed on 11 October 2022).
41. Beckman, W.A.; Klein, S.A.; Duffie, J.A. *Solar Heating Design, by the f-Chart Method*; Wiley: New York, NY, USA, 1977.
42. Deepika, D.; Baig, M.; Reddy, A.; Maneaih, D. Utilization of f-Chart Method for Designing Solar Thermal Heating System. *IOSR J. Mech. Civ. Eng.* **2016**, *16*, 23–28. [CrossRef]
43. IDAE. *Instalaciones de Energía Solar Térmica Pliego de Condiciones Técnicas de Instalaciones de Baja Temperatura*; Instituto para la Diversificación y Ahorro de la Energía: Madrid, Spain, 2009.
44. *ASHRAE Guidelines 14-2014*; Measurement of Energy and Demand Savings. American Society of Heating Refrigerating and Air-Conditioning Engineers: Atlanta, GA, USA, 2014.
45. ITeC (Instituto de la Tecnología de la Construcción de Cataluña). Available online: https://itec.es/servicios/bedec/ (accessed on 3 February 2021).

46. Casini, M. 7-Advanced insulation glazing. In *Smart Buildings*; Casini, M., Ed.; Woodhead Publishing: Cambridge, MA, USA, 2016; pp. 249–277.
47. Vanhoutteghem, L.; Skarning, G.C.J.; Hviid, C.A.; Svendsen, S. Impact of façade window design on energy, daylighting and thermal comfort in nearly zero-energy houses. *Energy Build.* **2015**, *102*, 149–156. [CrossRef]
48. Tam, V.W.Y.; Le, K.N.; Wang, J.Y. Cost Implication of Implementing External Facade Systems forCommercial Buildings. *Sustainability* **2018**, *10*, 1917. [CrossRef]